Article

Journal of
Nanoscience and Nanotechnology
Vol. 15, 3743–3749, 2015
www.aspbs.com/jnn

Synthesis of Bimetallic Ni–Cr Nano-Oxides as Catalysts for Methanol Oxidation in NaOH Solution

Yingying Gu*, Jing Luo, Yicheng Liu, Haihong Yang, Ruizhou Ouyang, and Yuqing Miao

College of Science and School of Environment and Architecture, University of Shanghai for Science and Technology, Shanghai 200093, China

Bimetallic Ni–Cr nano-oxide catalysts were synthesized by thermal decomposition method and were investigated as the anode electrocatalysts for the oxidation of methanol. The catalysts were characterized by X-ray diffraction and transmission electron microscopy. The electroactivity of the catalysts towards methanol oxidation in a solution containing 0.25 M NaOH and 1.0 M MeOH was examined using cyclic voltammetry and chronoamperometry. The results indicate that a mixture of rhombohedral-structured NiO and Cr_2O_3 nanocrystals generated at the calcination temperature of 500–700 °C while octahedral-structured spinel $NiCr_2O_4$ formed at higher temperature. The influence of metallic molar ratio on the electrocatalytic performance of the catalysts was studied. The Ni–Cr nano-oxides prepared at comparatively low temperature displayed significantly higher catalytic activity and durability in alkaline solution toward electrooxidation of methanol compared with the pure nano NiO. The results indicate a synergy effect between NiO and Cr_2O_3 enhancing the electrocatalytic properties of the bimetallic Ni–Cr nano-oxide catalysts. Meanwhile, $NiCr_2O_4$ hardly increased the activity and durability of the catalyst. In addition, the Ni–Cr catalyst also exhibited excellent stability and good reproducibility. Therefore, Ni–Cr nano-oxide catalyst may be a suitable and cheap electrocatalyst for methanol oxidation in alkaline medium.

Keywords: Direct Methanol Fuel Cell, Methanol Oxidation, Nano Oxide, Bimetallic Oxide.

1. INTRODUCTION

Direct methanol fuel cells (DMFCs) have been attracted much attention for its high theoretical energy density of methanol, using liquid fuel, working at low temperature, and have presented opportunities for use as a power source for portable electronic devices such as notebook computers, cellular phones.[1–3] Pt and Pt-based alloys have been proved to be highly efficient anode catalysts for fuel cells. However, the high cost and the apt to be poisoned by even trace CO originated from the oxidation of methanol prevent their practical applications in DMFCs.[4–6] Consequently, many attentions have been focused on the development of non-precious metal catalysts to overcome the technical barriers,[7–18] among which, nickel based materials are of the most promising candidates because of their good chemical stability, electrical properties and the ability of removing intermediate CO_{ad} in alkaline media.[19, 20] However, these catalysts still show much lower activity than the Pt catalysts. In order to improve the catalytic activity and durability, many research works have studied the modification of Ni-based catalysts through incorporating non-precious metallic elements, complexes and oxides. Ni–Pd nanoparticles,[21] Ni/TiO_2 nanotubes,[22] AuNi supported on carbon,[23] Au nanoparticle-coated Ni/Al layered double hydroxides,[24] Ni–Cd coated graphite[25] and Ni–Cu alloy[26] were investigated and showed enhanced electrocatalytic activity and stability for methanol oxidation reaction (MOR). According to the reports that the electroactivity of Ni-based catalysts depends mainly on the catalytic role of $Ni(OH)_2$/NiOOH redox as an effective electron transfer mediator for the oxidation process of alcohols, carbohydrates and many other organics in alkaline solutions.[27–31] The electrooxidation mechanisms on these catalysts involve the formation of a higher valence Ni oxide, which acts as a chemical oxidizing agent.

Herein, bimetallic Ni–Cr nano-oxide catalysts were synthesized by a thermal decomposition method in order to enhance the electrocatalytic performance of nickel-based catalyst for the oxidation of methanol in alkaline medium. The catalysts were characterized by X-ray diffraction

---

*Author to whom correspondence should be addressed.

(XRD) and transmission electron microscopy (TEM). The electrocatalytic properties of the Ni–Cr nano-oxides for MOR were studied by cyclic voltammetry and chronoamperometry. An attempt was made to determine the interrelation between the phase and chemical composition of the catalysts and their activities in methanol oxidation.

2. EXPERIMENTAL DETAILS

2.1. Preparation of Catalyst

Nafion solution (5.0%) was obtained from Shanghai Yibang technology Co., Ltd. All other chemicals used were of analytical grade and were used as received without any further purification from Sinopharm Chemical Reagent Co., Ltd.

The catalysts were synthesized via thermal decomposition method. A typical process is described as follows: a mixture containing 3.3–7.5 mM $NiCl_2 \cdot 6H_2O$, 2.5–6.7 mM $CrCl_3 \cdot 6H_2O$ and 5 mL deionized water was stirred for 5 minutes to obtain a homogeneous solution, followed by the addition of 10 mM citric acid monohydrate, 10.5 mM ethylenediaminetetraacetic acid disodium salt and 10 mL ammonium hydroxide into the above-prepared mixture. The solution was kept in a resistance furnace at 300 °C for 3 h to get a hardened gel, which was then grinded to powder. The powder was further calcined in the resistance furnace at 500 °C, 600 °C, 700 °C, 800 °C, 900 °C, respectively, for 2 h with a heating rate of 2 $°C \cdot min^{-1}$. Finally, the powder was washed with deionized water and dried in air. The obtained nano-oxide materials were then marked as Ni_a–Cr_b (a/b refers to the molar ratio of Ni/Cr).

2.2. Apparatus

The size and morphology of catalysts were observed using a TECNAI $G^2$20 (JEOL) transmission electron microscope operated at 200 kV. The X-ray powder diffraction patterns of the products were investigated with a Rigaku D/max 22009C/pc (Japan) diffractometer with CuKα radiation ($\lambda = 1.5406$ Å). The diffraction patterns were collected at room temperature by step scanning in the range of $10° \leq 2\theta \leq 90°$, at the scan rate of $2° \cdot min^{-1}$. All electrochemical experiments were carried out using a CHI660D electrochemical working station.

2.3. Electrochemical Measurements

Electrochemical measurements were performed using a three-electrode configuration consisting of a catalyst modified glass carbon (GC, $\Phi = 3$ mm), a Pt wire and a saturated calomel electrode (SCE) as working, counter and reference electrodes, respectively. Cyclic voltammograms (CVs) were recorded using a modulated potentiostat.

The GC electrodes were first polished to a mirror like surface using a standard electrode polishing kit and cleaned with acetone and distilled water successively. A mixture containing 20 mg catalyst, 2 mL ethanol and 10 μL 5% Nafion solution was dispersed ultrasonically for 15 min to obtain a well-dispersed ink suspension. 10 μL of the resulting suspension was then dropped onto the surface of GC electrode, which was dried at 30 °C for 15 min. For cyclic voltammetry experiments, the electrode was conditioned in an aqueous solution of 0.25 M NaOH and 1.0 M methanol at 30 °C by the potential cycling from 0 to 0.9 V (vs. SCE) at a scan rate of 100 $mV \cdot s^{-1}$ for 100 cycles.

3. RESULTS AND DISSCUSSION

3.1. Characterization of Ni–Cr Catalysts

TEM images of the Ni_1–Cr_1 samples calcined at different temperatures are shown in Figure 1. Well dispersed nanoparticles with size around 30 nm are obtained at the calcination temperature of 500 °C (Fig. 1(a)). The particle size increases as the increasing of calcination temperature and the prepared nanoparticles are almost spherical when the temperature is not higher than 700 °C (Figs. 1(b) and (c)). Much larger particles generate above 700 °C due to the surface fusion and congregation and a particle size range 100–900 nm is obtained. Clear crystalline facets with octahedral structure can be seen in Figures 1(d) and (e), indicating that the Ni_1–Cr_1 samples may be transformed into the spinel structure.[32, 33]

Figure 2 shows the XRD patterns of Ni_1–Cr_1 nano-oxides obtained at different calcination temperatures. The peaks in the patterns indicate that the Ni_1–Cr_1 nano-oxides obtained from the temperature between 500 °C and 700 °C are the mixtures of the crystalline NiO and Cr_2O_3.[34] The diffraction peaks at 2θ values of 37.3°, 43.3°, 62.9°, 75.4° and 79.4° are corresponding to the NiO with a rhombohedral structure. And the diffraction peaks at 2θ values of 24.5°, 33.6°, 36.3°, 41.5°, 43.3°, 50.3°, 54.9° and 65.2° are ascribed to the rhombohedral-structured Cr_2O_3. The average particle sizes calculated from the Scherer formula are about 28.9 nm, 31.4 nm and 38.5 nm at the calcination temperatures of 500 °C, 600 °C and 700 °C, respectively. The Ni_1–Cr_1 materials obtained at higher temperature have the comparatively larger crystal sizes because of more energy for the crystal growing stage.[32] Characteristic peaks of spinel-structured $NiCr_2O_4$ are observed in the XRD pattern with decreasing intensities of Cr_2O_3 and NiO at the temperature of 800 °C indicating the inset of NiO into the lattice of Cr_2O_3. The characteristic peaks of Cr_2O_3 almost disappear at 900 °C, which means that the mixture has been almost completely transformed into nickel chromite spinel after the thermal process. The formation mechanism can be expressed by the following chemical reaction:[35, 36]

$$Cr_2O_3 + NiO \rightarrow NiCr_2O_4$$

3.2. Electrocatalytic Performance of Ni–Cr Catalysts for Oxidation of Methanol

A consecutive sweep from 0 to 0.9 V was conducted for 100 cycles on Ni_1–Cr_1 electrode in alkaline solution.

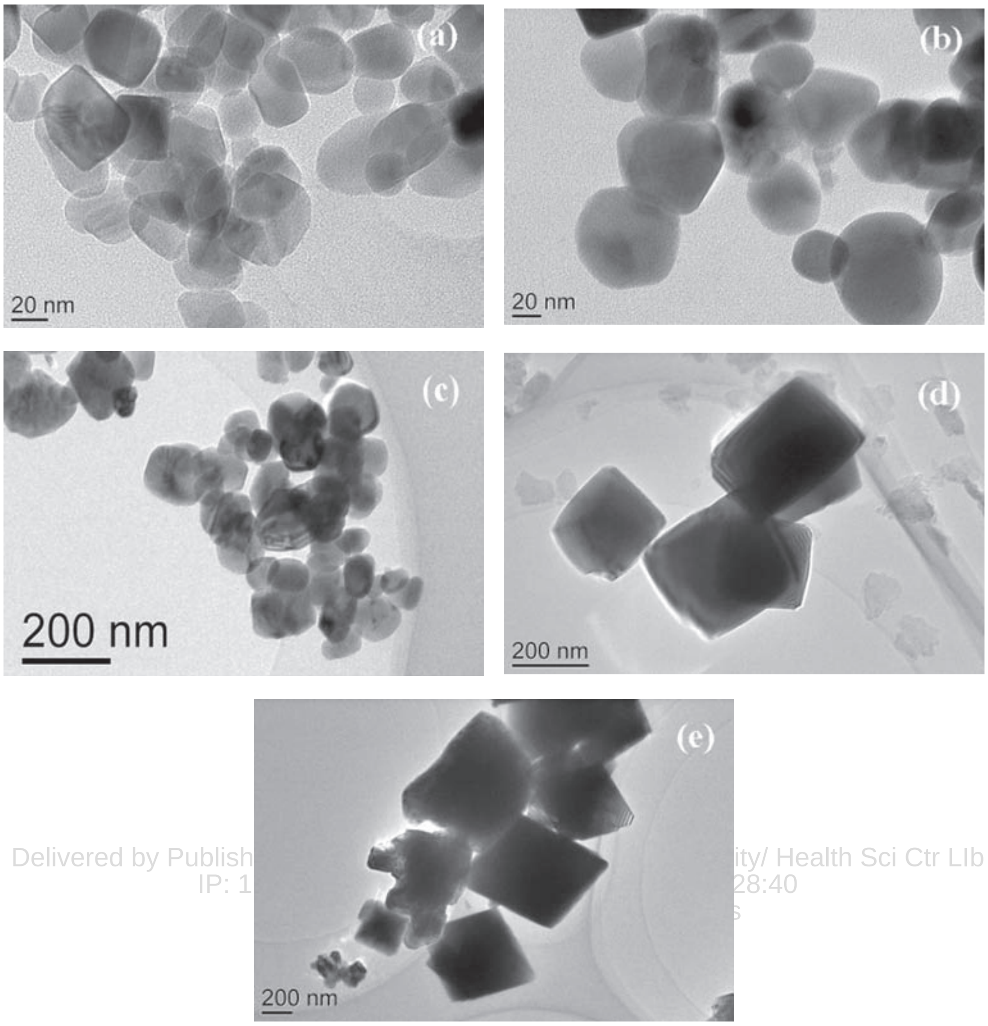

Figure 1. TEM images of Ni_1–Cr_1 nano-oxides calcined at (a) 500 °C, (b) 600 °C, (c) 700 °C, (d) 800 °C and (e) 900 °C.

Figure 3 shows that the peak current density increases with increasing scan cycle within 50 cycles and thereafter, no obvious changes are found in the oxidation potential and maximal current density with more scan cycle done. The CV curves between 50th and 100th scan cycle are almost overlapped. Therefore, the CV data of the 100th cycle are present in the following CV figures.

In the consecutive CVs of Ni_1–Cr_1 catalyst, except the first cycle, the peak potentials are almost invariable, suggesting that the phase transformation of Ni oxyhydroxide from β to γ is inhibited.[26] It is reported that there are four phase produced over the lifetime of a nickel hydroxide electrode substrate, namely, β-$Ni(OH)_2$, α-$Ni(OH)_2$, β-NiOOH and γ-NiOOH.[37,38] It has been identified that phase transformations are likely to occur during a normal cycle. β-$Ni(OH)_2$ is first oxidized to β-NiOOH and reduced back during the cell discharge. Meanwhile, the reduction of γ-NiOOH forms the hydrated α-$Ni(OH)_2$ phase, which is unstable in strong alkali and ages to the β-form.[39] It is well-known that the formation of γ-NiOOH phase is associated with swelling or volume expansion of nickel film electrodes leading to the subsequent microcracks and disintegration of the nickel film. Lower inter-electrode spacing results in lower internal resistance and thus better efficiency of the electrode. Therefore, β-NiOOH phase is considered to be a better electroactive material for high electrochemical performance in alkaline solution. Thus, the peak current density of the Ni_1–Cr_1 electrode increases continuously before the 50th round can be ascribed to the consecutively formation of β-NiOOH from γ-NiOOH.

The CV behaviours of Ni_1–Cr_1 nano-oxide catalysts calcined at different temperatures are shown in Figure 4. Peaks for MOR appear at around 0.66 V (vs. SCE) of Ni_1–Cr_1 catalysts, while no significant peak is observed under the same condition for bare GC electrode. Therefore, the peaks can be attributed to the catalytic oxidation of methanol by Ni_1–Cr_1 nano-oxides in alkaline solution. And the current density for MOR on Ni_1–Cr_1 calcined at 700 °C is higher than that at 500 and 600 °C owing to the higher crystallinity of the catalysts, which is evidenced by sharper peaks at higher decomposition temperature in the

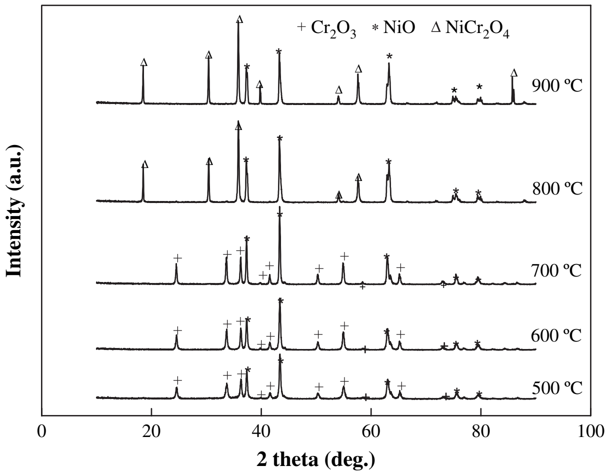

Figure 2. XRD patterns of Ni_1–Cr_1 nano-oxides calcined at different temperatures.

XRD patterns.[25, 40] On the other hand, in the cases of the samples calcined at 800 and 900 °C, the peak current densities are quite lower than the others, due to the formation of $NiCr_2O_4$ with large sizes. It is obvious that the mixture of Cr_2O_3 and NiO nanoparticles exhibites a higher activity toward methanol oxidation in comparison with $NiCr_2O_4$, which indicates Cr_2O_3 is a good promoter of the Ni–Cr catalysts for MOR, while $NiCr_2O_4$ can hardly increase the catalytic activities of the catalysts.

The peak current ratio of the forward scan (I_f) to backward scan (I_b) has generally been used to evaluate the poisoning tolerance for methanol oxidation.[41] The higher I_f/I_b ratio indicates more effective removal of the poisoning species on the catalyst surface, thus the better tolerance toward poisoning of the catalyst.[42] The I_f/I_b ratios of Ni_1–Cr_1 nano-oxides are shown in Table I. Among these samples, Ni_1–Cr_1 calcined at 700 °C has a high I_f/I_b value of 1.29, which is higher than that of Pt/C (0.92),[33] and even higher than that of Pt–Co nanowire catalyst (1.20)[43] and porous Pt–Ni nanotubes (1.26).[44] This comparatively higher value of I_f/I_b for Ni_1–Cr_1 catalyst indicates the highly active and resistant to the poisoning of carbonaceous species. Obviously, the catalysts calcined at relatively lower temperature show higher current densities as well as higher I_f/I_b values than the samples calcined above 800 °C, suggesting that the catalysts containing both NiO and Cr_2O_3 have a higher resistant to the poison carbonaceous species than $NiCr_2O_4$.

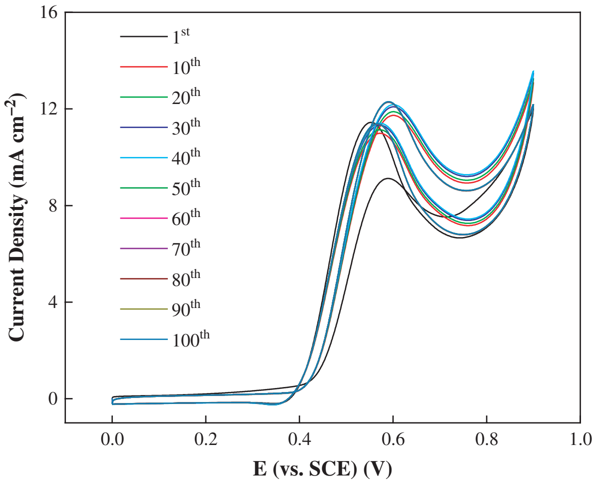

Figure 3. CVs of Ni_1–Cr_1 electrode for 100 consecutive cycles in 0.25 M NaOH and 1.0 M methanol solution at the scan rate of 100 mV · s^{-1} at 30 °C.

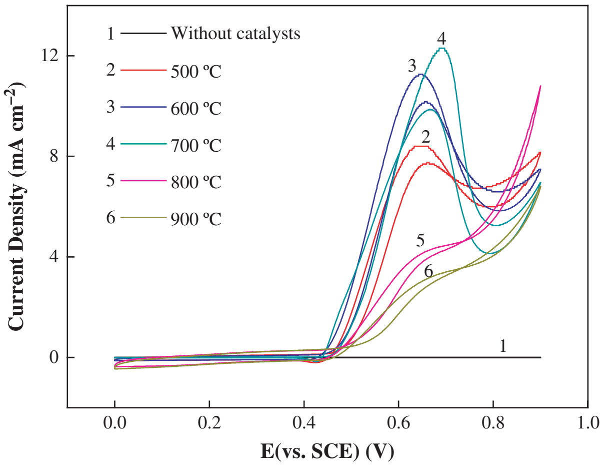

Figure 4. CVs of Ni_1–Cr_1 nano-oxides prepared at different calcination temperatures in 0.25 M NaOH and 1.0 M methanol solution at the scan rate of 100 mV · s^{-1} at 30 °C.

The CVs of Ni–Cr nano-oxides with different metallic molar ratios toward MOR are shown in Figure 5. Here, the electroactivity of monometallic nano-oxides, pure NiO and Cr_2O_3, was also tested for methanol oxidation, which were synthesised using the same method as Ni–Cr nano-oxides. All catalysts show electroactivity for MOR, while the pure nano-Cr_2O_3 is the poorest catalyst among all the samples and catalytic peak current density of pure nano-NiO is also much lower than that of the Ni–Cr nano-oxides. Notably, the catalytic oxidation peak current density exhibited by Ni–Cr nano-oxides are even much higher than the sum of peak current densities given by the pure nano-Cr_2O_3 and the pure nano-NiO, and the highest one is found at the molar ratio of 2:1 as listed in Table II. The results reveal the higher electrocatalytic activity of the bimetallic Ni–Cr nano-oxides toward methanol oxidation than the

Table I. Electrocatalytic properties of Ni_1–Cr_1 nano-oxides prepared at different calcination temperatures.

Sample (°C)	Peak current density (mV · cm^{-2})	I_f/I_b
500	8.3	1.11
600	11.5	1.14
700	12.6	1.29
800	4.2	1.06
900	3.5	1.05

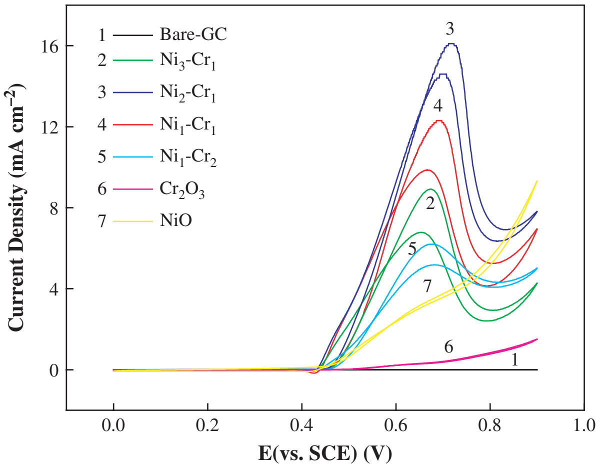

Figure 5. CVs of Ni–Cr nano-oxides with different molar ratio of Ni/Cr in 0.25 M NaOH and 1.0 M methanol solution at the scan rate of 100 mV · s^{-1} at 30 °C.

monometal oxide catalyst of NiO or Cr_2O_3 due to the significant synergy effect of NiO and Cr_2O_3.

In the electrochemical process, the β-Ni(OH)$_2$ of the electrodes is oxidized to β-NiOOH in low potential and transformed to γ-NiOOH in high potential during the positive sweep. Then methanol is oxidized on the electrode surface by the intermediate product NiOOH. The comparison of the electrochemical behaviour between the pure nickel oxide and Ni–Cr oxide reveals the lower α/γ redox contribution with a good stabilization of β/β nickel oxyhydroxide form on the Ni–Cr electrode. This is due to the inhibition of variation of peak potentials after prolonged electrochemical treatment in alkaline solution. Thus the addition of chromium to the nickel oxyhydroxide species represents a very efficient strategy to suppress the formation of γ-NiOOH phase. Additionally, the presence of Cr_2O_3 nanoprticles enhances the formation of Ni^{III}/Ni^{II} redox couple, therefore, the catalytic activity and mechanical stability are improved.[45,46] Similar electrochemical behaviour was observed for alloys obtained by adding several percent of Cd, Zn, Co, Ca, Ti and other elements to the nickel hydroxide.[26,47,48]

The peak current densities and the I_f/I_b ratios show interesting differences between the catalysts in Table II. All the Ni–Cr electrodes exhibit much higher I_f/I_b ratios than the pure Cr_2O_3 and NiO electrodes, highlighting their strongly reduced poisoning and hence improved stability,[49] which may be attributed to the enhancement of the oxidation of CO by Cr atom.[36]

Table II. Electrocatalytic properties of Ni–Cr nano-oxides with different molar ratio of Ni/Cr.

Sample	Peak current density (mV · cm^{-2})	I_f/I_b
Ni_3–Cr_1	9.2	1.27
Ni_2–Cr_1	16.0	1.14
Ni_1–Cr_1	12.6	1.29
Ni_1–Cr_2	6.3	1.19
NiO	3.1	1.05
Cr_2O_3	0.9	1.03

CVs of Ni_1–Cr_1 electrode at different scan rates and the plot of I_f against the square root of the scan rates are shown in Figures 6(a) and (b). The catalytic oxidation peak potentials of methanol shift gradually towards more positive values with increasing scan rate, suggesting a kinetic limitation on surface diffusion of methanol. A linear dependence of I_f on the square root of the scan rate is observed, conforming that the electrocatalytic oxidation of methanol at the Ni_1–Cr_1 electrode is controlled by a semi-infinite linear diffusion process.

Reproducibility was tested by measuring CVs of 5 independently prepared Ni_1–Cr_1 electrodes in 0.25 M NaOH containing 1.0 M methanol, as shown in Figure 7. A relative standard deviation (RSD) of 0.72% is estimated for the oxidation peak currents, which indicates good fabrication reproducibility. The stability of the electrode was also studied. The electrode employed in this measurement was kept in room temperature and repeated assays every day in 9 days, as shown in Figure 8. The response signal retained 93.9% of the initial one after 9 days and the RSD

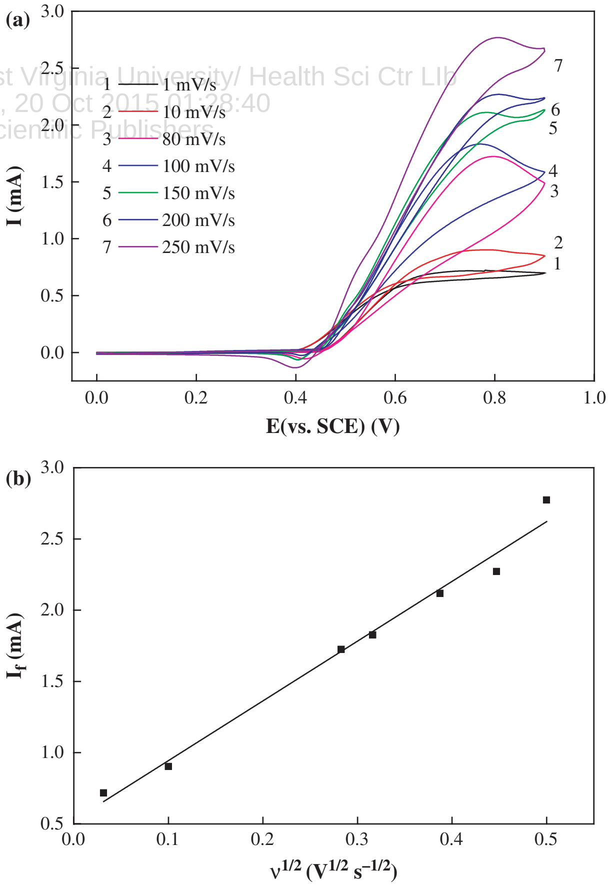

Figure 6. (a) CVs of Ni_1–Cr_1 nano-oxides in 0.25 M NaOH and 1.0 M methanol solution at the scan rate of 1, 10, 80, 100, 150, 200, 250 mV · s^{-1}, (b) Plot of I_f versus $v^{1/2}$.

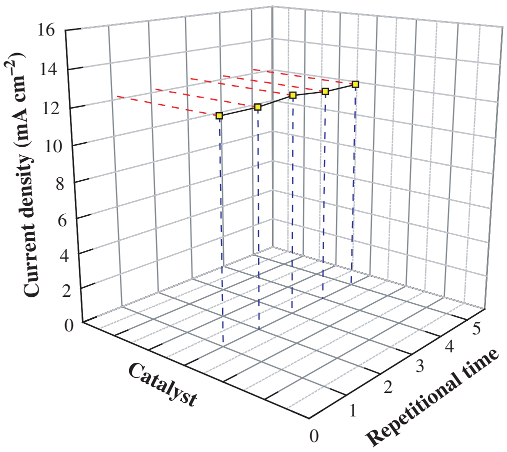

Figure 7. Results of five repetitive measurements of Ni_1–Cr_1 electrode in 0.25 M NaOH and 1.0 M methanol solution at the scan rate of 100 mV · s^{-1} at 30 °C.

is calculated to be 2.0%, reflecting a good stability of the electrode.

Figure 9 shows the chronoamperometric curve for MOR on the Ni_1–Cr_1 electrode in alkaline solution. The initial high current density mainly corresponds to the double-layer charging. The electrode presents continuous decay in activity during the first few minutes, which can be attributed to the remaining of the adsorbed intermediate products of methanol oxidation such as CO poisoning on the surface of electrode.[50,51] And the current density behaves a more stable trend through a long time testing, owing to the adsorption of OH^-, which may help to diminish CO poisoning and also facilitate the oxidation of MeOH to $HCOO^-$ and CO_2.[52] Accordingly, these results illustrate that the Ni–Cr catalyst display favorable stability, high catalytic activity and high anti-poisoning ability for methanol oxidation, in good agreement with the CV results.

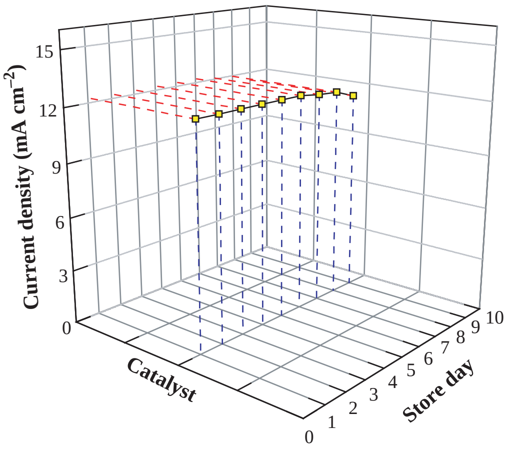

Figure 8. Changes in current density of Ni_1–Cr_1 electrode with the store day in 0.25 M NaOH and 1.0 M methanol solution at the scan rate of 100 mV · s^{-1} at 30 °C.

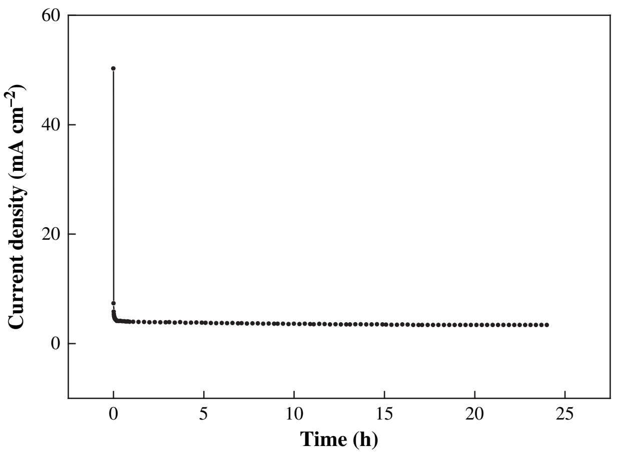

Figure 9. Chronoamperometric curve of Ni_1–Cr_1 electrode in 0.25 M NaOH and 1.0 M methanol solution, applied potential 0.67 V.

4. CONCLUSIONS

Ni–Cr electrocatalysts for MOR with different molar ratios have been synthesized via the thermal decomposition synthesis process. The XRD and TEM characterizations indicate that the bimetallic Ni–Cr nanoparticles are well dispersed with average particle size of about 30–40 nm below 700 °C. The electrochemical measurements show that the Ni–Cr nano-oxides calcinated at 700 °C exhibit remarkably high activity towards methanol oxidation in alkaline media. Meanwhile, good stability is observed over a moderately extended period. The values of current density and I_f/I_b for Ni_1–Cr_1 electrode are 12.6 mV · cm^{-2} and 1.29, respectively. The kinetic results indicate that the reaction of the electrooxidation of methanol is a diffusion-controlled process. The relatively high current density, high CO tolerance as well as stability suggest that the Ni–Cr nano-oxides may act as a promising catalyst for DMFCs in alkaline media.

Acknowledgment: The authors greatly appreciate the support from the Shanghai Committee of Science and Technology (No. 11430502100), the National Natural Science Foundation of China (No. 21305090), the Natural Science Foundation of Shanghai (No. 13ZR1428300) and the Innovation Program of Shanghai Municipal Education Commission (Nos. 14ZZ139, 14YZ086).

References and Notes

1. J. Y. Park, J. H. Kim, Y. Seo, D. J. Yu, H. Cho, and S. J. Bae, *Fuel Cells* 12, 426 **(2012)**.
2. Q. Z. Lai, G. P. Yin, and Z. B. Wang, *Int. J. Energy Res.* 33, 719 **(2009)**.
3. Y. Paik, S. S. Kim, and O. H. Han, *Angew. Chem. Int. Ed.* 47, 94 **(2008)**.
4. J. Tan, J. H. Yang, X. H. Liu, F. Yang, X. Y. Li, and D. Ma, *Electrochem. Commun.* 27, 141 **(2013)**.
5. H. Yano, M. Kataoka, H. Yamashita, H. Uchida, and M. Watanabe, *Langmuir* 23, 6438 **(2007)**.

6. T. Ghosh, B. M. Leonard, Q. Zhou, and F. J. DiSalvo, *Chem. Mater*. 22, 2190 **(2010)**.

7. M. R. Gao, Q. Gao, J. Jiang, C. H. Cui, W. T. Yao, and S. H. Yu, *Angew. Chem*. 123, 5007 **(2011)**.

8. Z. B. Wang, C. R. Zhao, P. F. Shi, Y. S. Yang, Z. B. Yu, W. K. Wang, and G. P. Yin, *J. Phys. Chem. C* 114, 672 **(2009)**.

9. W. Li, Q. Xin, and Y. Yan, *Int. J. Hydrogen Energy* 35, 2530 **(2010)**.

10. S. J. Liu, *Electrochim. Acta*. 49, 3235 **(2004)**.

11. K. Ren and Y. X. Gan, *Adv. Sci. Eng. Med*. 5, 811 **(2013)**.

12. Q. Yi, W. Huang, J. Zhang, X. Liu, and L. Li, *Catal. Commun*. 9, 2053 **(2008)**.

13. M. A. Abdel Rahim, R. M. Abdel Hameed, and M. W. Khalil, *J. Power Sources* 134, 160 **(2004)**.

14. J. Khera, A. Singh, S. K. Mandal, and A. Chandra, *Adv. Sci. Eng. Med*. 5, 1067 **(2013)**.

15. A. M. Prasad, C. Santhosh, K. Priya, and A. N. Grace, *Adv. Sci. Eng. Med*. 5, 395 **(2013)**.

16. M. H. Koo and H. H. Yoon, *J. Nanosci. Nanotechnol*. 13, 7434 **(2013)**.

17. R. Vinodh and D. Sangeetha, *J. Nanosci. Nanotechnol*. 13, 5522 **(2013)**.

18. N. V. Long, C. M. Thi, Y. Yong, M. Nogami, and M. Ohtaki, *J. Nanosci. Nanotechnol*. 13, 4799 **(2013)**.

19. Q. Jiang, L. Jiang, H. Hou, J. Qi, S. Wang, and G. Sun, *J. Phys. Chem. C* 114, 19714 **(2010)**.

20. C. S. Chen, F. M. Pan, and H. J. Yu, *Appl. Catal. B* 104, 382 **(2011)**.

21. Y. Zhao, X. Yang, J. Tian, F. Wang, and L. Zhan, *Int. J. Hydrogen Energy* 35, 3249 **(2010)**.

22. H. He, P. Xiao, M. Zhou, Y. Zhang, Q. Lou, and X. Dong, *Int. J. Hydrogen Energy* 37, 4967 **(2012)**.

23. S. Yan, L. Gao, S. Zhang, L. Gao, W. Zhang, and Y. Li, *Int. J. Hydrogen Energy* 38, 12838 **(2013)**.

24. Y. Wang, H. Ji, W. Peng, L. Liu, F. Gao, and M. Li, *Int. J. Hydrogen Energy* 37, 9324 **(2012)**.

25. A. Döner, E. Telli, and G. Kardas, *J. Power Sources* 205, 71 **(2012)**.

26. I. Danaee, M. Jafarian, F. Forouzandeh, F. Gobal, and M. G. Mahjani, *Int. J. Hydrogen Energy* 33, 4367 **(2008)**.

27. G. Y. Choi, Y. C. Kim, D. J. Moon, G. Seo, and N. C. Park, *J. Nanosci. Nanotechnol*. 13, 653 **(2013)**.

28. Y. Miao, J. Wu, S. Zhou, Z. Yang, and R. Ouyang, *J. Electrochem. Soc*. 160, B47 **(2013)**.

29. K. Dhanapalan, S. S. Gwan, J. M. Dong, H. K. Jong, C. P. Nam, and C. K. Young, *J. Nanosci. Nanotechnol*. 11, 1443 **(2011)**.

30. J. W. Kim and S. M. Park, *J. Korean Chem. Soc*. 8, 117 **(2005)**.

31. T. R. Kumar, J. J. Vijaya, and J. L. Kennedy, *J. Nanosci. Nanotechnol*. 13, 2953 **(2013)**.

32. N. H. Li, Y. H. Chen, C. Y. Hu, C. H. Hsieh, and S. L. Lo, *J. Hazard. Mater*. 198, 356 **(2011)**.

33. X. D. Cheng, J. Min, Z. Q. Zhu, and W. P. Ye, *Int. J. Miner. Metall. Mater*. 19, 173 **(2012)**.

34. I. Tamiolakis, I. N. Lykakis, A. P. Katsoulidis, M. Stratakis, and G. S. Armatas, *Chem. Mater*. 23, 4204 **(2011)**.

35. M. Ahmad, C. Pan, Z. Luo, and J. Zhu, *J. Phys. Chem. C* 114, 9308 **(2010)**.

36. E. Antolini, J. R. C. Salgado, L. G. R. A. Santos, G. Garcia, E. A. Ticianelli, E. Pastor, and E. Gonzalez, *J. Appl. Electrochem*. 36, 355 **(2006)**.

37. H. Bode, K. Dehmelt, and J. Witte, *Electrochim. Acta*. 11, 1079 **(1966)**.

38. R. S. S. Guzman, J. R. Vilche, and A. J. Arvia, *J. Electrochem. Soc*. 125, 1578 **(1978)**.

39. D. J. Singh, *J. Electrochem. Soc*. 145, 116 **(1998)**.

40. S. M. Golabi and A. Nozad, *Electroanal*. 16, 199 **(2004)**.

41. X. Ge, R. Wang, P. Liu, and Y. Ding, *Chem. Mater*. 19, 5827 **(2007)**.

42. M. Cao, D. Wu, S. Gao, and R. Cao, *Chem. Eur. J*. 18, 12978 **(2012)**.

43. K. W. Park, J. H. Choi, B. K. Kwon, S. A. Lee, Y. E. Sung, H. Y. Ha, S. A. Hong, H. Kim, and A. Wieckowski, *J. Phys. Chem. B* 106, 1869 **(2002)**.

44. C. H. Cui, H. H. Li, and S. H. Yu, *Chem. Sci*. 2, 1611 **(2011)**.

45. Y. Miao, L. Ouyang, S. Zhou, L. Xu, Z. Yang, M. Xiao, and R. Ouyang, *Biosens. Bioelectron*. 53, 428 **(2014)**.

46. H. B. Hassan and Z. A. Hamid, *Int. J. Hydrogen Energy* 36, 5117 **(2011)**.

47. P. F. Luo, T. Kuwana, D. K. Paul, and P. M. A. Sherwood, *Anal. Chem*. 68, 3330 **(1996)**.

48. J. Chen, D. H. Bradhurst, S. X. Dou, and H. K. Liu, *J. Electrochem. Soc*. 146, 3606 **(1999)**.

49. S. Sharma, A. Ganguly, P. Papakonstantinou, X. Miao, M. Li, J. L. Hutchison, M. Delichatsios, and S. J. Ukleja, *J. Phys. Chem. C* 114, 19459 **(2010)**.

50. M. Zhiani, B. Rezaei, and J. Jalili, *Int. J. Hydrogen Energy* 35, 9298 **(2010)**.

51. Y. Zhao, F. Wang, J. Tian, X. Yang, and L. Zhan, *Electrochim. Acta* 55, 8998 **(2010)**.

52. J. L. Cohen, D. J. Volpe, and H. D. Abruna, *Phys. Chem. Chem. Phys*. 9, 49 **(2007)**.

Received: 19 November 2013. Accepted: 11 January 2014.